Article

Optimal Combination Design of a Light Emitting Diode Matrix Applicable to a Flyback Drivers

Ming-Chang Tsou [1,*], Ming-Tes Kuo [2]

1 Leadtrend Technology Corporation, No.1, Taiyuan 2nd St., Zhubei City, Hsinchu County, Taiwan; ming@leadtrend.com.tw (M.-C.)
2 Department of Electrical Engineering, National Taiwan University of Science and Technology, No.43, Section 4, Keelung Road, Da'an District, Taipei 106, Taiwan; mkuo@mail.ntust.edu.tw (M.-T.)

Abstract: The present study analyzed light emitting diodes (LEDs) as an output load and used a Taylor series to describe the characteristic curve based on the exponential characteristic of voltage and current. A prototype circuit of a flyback LED driver system was established to verify whether the theory is consistent with actual results. This study focused on the exponential relationship of LED voltage and current. Conventional simulations usually used linear models to present LED loads. However, the linear model resulted in considerable error between simulation and actual characteristics. Therefore, this study employed a Taylor series to describe the nonlinear characteristic of an LED load. Through precise calculations with Mathcad computation software, the error was effectively reduced. Moreover, the process clarified the influence of temperature on LEDs, which benefited the characteristic analysis of the entire system. Finally, a realized circuit of 120-W flyback LED drivers was established for conducting theory verification, including theoretic analysis and evaluation of the system design process of the flyback converter. The circuit simulation software SIMPLIS was used to demonstrate the system model, which enabled quick understanding of the system framework established in this study. Regarding LEDs, a commercially available aluminum luminaire was used as the output load. The measured results of the actual circuit and the simulation results were remarkably consistent. For the same system at the same temperature, the error between the simulation and actual results was less than 3%, which proved the reliability of the Taylor series simulation.

Keywords: Flyback, LED; Flicker; Light-Emmitting-Diode; Taylor Series

PACS: J0101

1. Introduction

Continual technological developments have improved human living environments and the convenience of performing everyday activities. However, technological developments have resulted in substantial energy consumption. In recent years, because of problems such as the progression of global warming and energy shortages, people have become increasingly aware of the importance of environmental protection. Therefore, the demands for energy conservation and highly efficient products have increased. Light emitting diode (LED) technology, which has been undergoing development since 1962[1], has reached a certain level of maturity. Because of their numerous merits and unique features, LEDs have gradually replaced conventional light sources and become the primary light source of this era.

The fluorescent tubes used in fluorescent lamps have an unstable and flickering lighting source, which may cause dangers in certain working environments [2], [3]. Such unstable light sources cause fatigue for human eyes. Moreover, the mercury contained in fluorescent tubes is harmful for the human body and the environment. In addition, conventional incandescent light bulbs and

halogen lamps feature short life expectancy, low efficiency, high power consumption, and high levels of heat generation, which may be considered to incur excessive energy consumption [4], [5].

Technological developments have led to changes in the lighting source, luminaire, control, and design of lighting products that have greatly improved their efficiency. Additionally, the establishment of energy-saving indices and government policies has created further room for improvement in terms of energy-saving characteristics, particularly regarding LED application. The energy consumption of luminescence in LED luminaire systems is remarkably lower than that of conventional light sources such as incandescent light bulbs and fluorescent lamps. The luminescence efficiency of regular high-brightness LED luminaires corresponds to 50% less energy consumption than fluorescent lamps and 85% less than that of incandescent light bulbs [6]. Therefore, adopting energy-saving illumination products to replace conventional ones can achieve optimal energy-saving outcomes and the ultimate goal of energy conservation.

LEDs are driven by direct current (DC) voltage. An alternating current (AC)–DC power factor correction (PFC) converter must be applied for regular grid power to be used for LED light sources. However, for the driver, LEDs perform a nonlinear load, and the current–voltage (I–V) curve can be presented as exponential function in Equation. 1. Compared with a regular linear load, a nonlinear load is more difficult for users to design; the curvature increases the possibility of errors between simulation and practice (Fig. 1) [7]. Applying the linear model to conduct simulation and design will result in notable differences from the actual LED curve. Therefore, the objective of this study was to determine a simulation method that enables the researcher to obtain data similar to actual ones without going through complex measuring processes as well as minimize the discrepancy between simulation and actual data.

$$I_{LED} = I_{sat}(e^{\frac{q \cdot V_{LED}}{k \cdot T}} - 1) \qquad (1)$$

I_{LED} : forward current; V_{LED} : forward voltage.

I_{sat} : saturation current or critical current of the diode.

q : number of the electric charges of the electron (=1.62 • 10^{-19}).
k : the Boltzmann constant (=1.38 • 10^{-23}).
T : absolute temperature (=273 + room temperature).

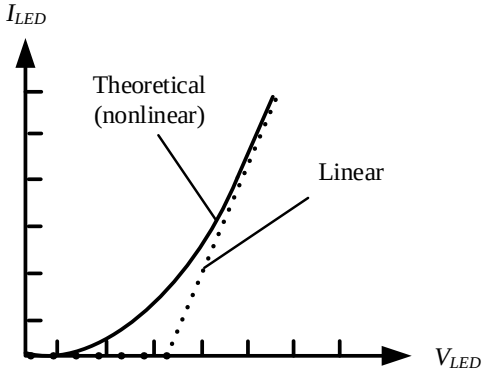

Figureure 1. Schematic of low-frequency Ripples

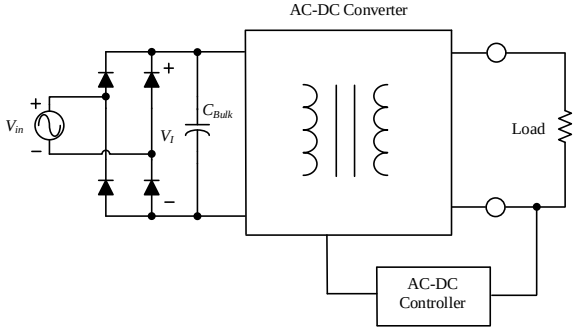

Figureure 2. Flyback Converter Framework

Although the energy-saving performance of LED light sources is superior to that of conventional light sources, specific voltage-converting equipment is required in order to achieve the rated voltage and current required for LEDs to function properly. In addition, different LED luminaires are equipped with different converters. The use of an adequate and highly efficient LED power converter is critical. Fig. 2 presents the framework of the flyback converter used in this study. The PFC circuit is added to the first stage because most modern electrical appliances have nonlinear loads, which result in phase angle deviation between the input voltage and input current and causes a reduction in the power factor. In addition, the input current generates an enormous amount of harmonic waves after a bridge rectification. The power supply quality and system efficiency tend to be low under the influence of low power factor and large amounts of harmonic waves. Therefore, existing power supplies and drivers on the market are equipped with PFC circuits to suppress harmonic waves of the current and increase the power factor to prolong the life expectancy [8].

The present study investigated the optimal combination design of the LED matrix applicable to the flyback driver. This study also serves as a step-by-step guide for readers, from theory-induction to circuit design and Taylor series simulation analysis of loads, for effectively and quickly understanding this research and reducing the time required for the design process.

2. Single-stage PFC Circuit

2.1. Boundary Conduction Current Mode Control

The circuit and relevant waveforms of voltage mode control (VMC) [9], [10], [11] are presented in Figs. 3 and 4. The bandwidth of the error amplifier (E/A) is also set remarkably lower than the frequency of input voltage, and V_{EA} is a DC voltage with extremely low ripples. After comparing the reference voltage V_{ref} with the feedback voltage V_{FB}, which is obtained at the output end V_O by dividing the voltage by resistances, the E/A is employed to obtain the amplified DC signal V_{EA}, which is drawn to compared with V_{Rampr} (Fig. 3). When $V_{Rampr} < V_{EA}$, the power switch is on and the inductor is storing energy; whereas when the voltage V_{Rampr} increases to $\geq V_{EA}$, the R end of the RS flip-flop is instantly triggered to turn the power switch off and the inductor begins to release energy. Till the energy stored in the inductor runs out, the zero current detector (ZCD) circuit sends a wake-up signal V_{ZCD} to the S end of the RS flip-flop. Next, the RS flip-flop Q outputs a high-level signal to turn the switch back on. This action is repeated to achieve output voltage stabilization and regulation as well as high power factor. This method employs variable-frequency control in which a constant on-time (COT) is retained and the switching frequency varies with the input voltage and output load. The cost of VMC is lower because the multiplier is needless. In addition, the current sensing resistance in VMC is reserved simply for over-current protection.

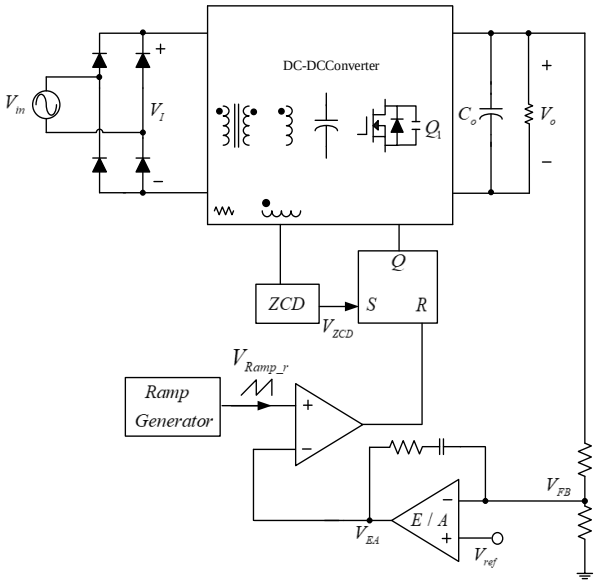

Figureure 3. Block Diagram of the VMC Circuit

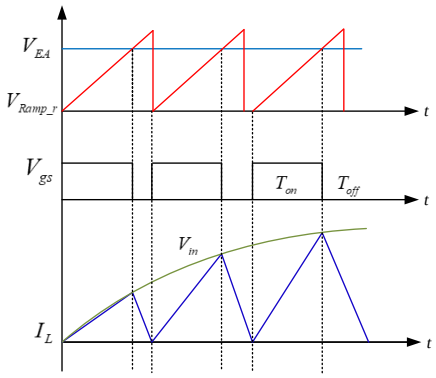

Figureure 4. Voltage Signal of the VMC

2.2. Main Device Parameter Design

The system framework established in this study is the 120-W flyback LED driving circuit (Fig. 5). The specifications of this framework are listed in Table 1.

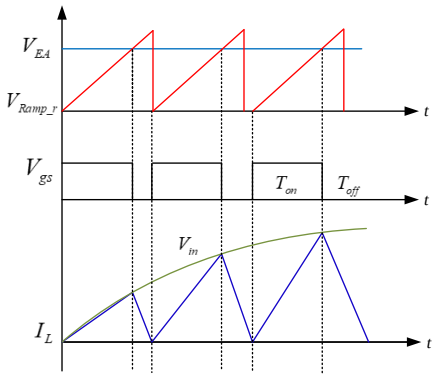

Figureure 5. Voltage Signal of the VMC

Table 1. System Parameters and Specifications

Hardware Parameter Setting	Specifications
Input voltage V_{in} *(ac)*	85V~265V
Maximum output voltage V_O	12V
Maximum output current I_O	10A
Minimum full-load switching frequency $f_{s\min}$	50kHz

1) Selection of the MOSFET Power Switch Q_1

The selection of the MOSFET concerns the setting of transformer turn ratio n, which is a trade-off condition; that is, a higher n corresponds to a higher power factor and lower total harmonic distortion (THDs). However, as shown in (2), a higher n corresponds to greater stress of the drain–source voltage $V_{ds\max}$ on the switch and consequently incurring greater cost.

$$V_{ds\max} = \sqrt{2}V_{in\max} + nV_O + \Delta V \qquad (2)$$

$V_{in\max}$: the maximum effective value of the input voltage;

ΔV : the voltage of the leakage inductance effect, which is usually set at half of the mapped voltage V_{R} .(From output voltage).

By the way, the endurance of the maximum conducting current of the switch, $\mathrm{I}_{ds\max} = I_{peakP}$, must also be taken into consideration.

2) Selection of the Secondary-Side Output Rectifier Diode D_S

A higher n corresponds to a lower reverse voltage of the secondary-side diode $V_{Dioder(\max)}$, as indicated in (3).

$$V_{Dioder(\max)} = \frac{\sqrt{2}V_{in\max}}{n} + V_O \qquad (3)$$

The endurance of the maximum conducting current of the secondary side $I_{D\max} = nI_{peakP}$ must also be taken into consideration when choosing the rectifier diode.

3) Selection of the Bridge Rectifier B

The input voltage of a bridge rectifier is a low-frequency signal; therefore, devices with high-frequency features are not required. Generally, only the peak input voltage and peak input current must be considered.

4) Selection of the Input Capacitor C_{BULK}

The most commonly selected input capacitor C_{BULK} is 1 μF or lower, which performs as a high-frequency filter capacitor rather than a rectifier; therefore, the capacitance is regarded as highly resistant for the input power frequency. Consequently, the voltage signal of C_{BULK} after bridge rectification forms an M-shaped wave.

5) Selection of the Output Capacitor C_O

Because the output voltage ripple of the output capacitor C_O is twice the input power frequency, the capacitance of the PFC circuit established in this study is greater than that of a regular flyback converter and is given by (4):

$$C_O = \frac{I_{OMAX}}{2 \cdot \pi \cdot f_L \cdot \Delta V_{out}} \quad (4)$$

ΔV_{out} : the ripple voltage, which is usually set with a peak-to-peak value of 1 V;

f_L : the input power frequency;

$I_{O\max}$: the maximum output current.

The output capacitor can be connected in parallel to reduce the equivalent series resistance and the output ripples.

According to the calculation, the specifications and parameters of the main devices are provided in Table 2.

Table 2. Parameters and Specifications Of The Main Devices Selected For The Circuit

Element	Specification	Model
Bridge rectifier B	600V/8A	GBU806
Input capacitor C_{BULK}	120μF/400V	Electrolytic capacitor
Output capacitor C_O	2040μF/25V	Electrolytic capacitor
Power switch MOSFET (Q_1)	600V/13A	2SK3797
Secondary side output diode D_S	200V/0.25A	BAS21

3. Simulation Of A Taylor Series [12], [13], [14], [15], [16]

Fig. 6 presents the single-stage LED model and Fig. 7 presents the I–V curve of the maximum and minimum operating point of the LED, which help to derive the Taylor series.

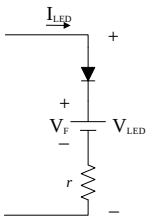

Figureure 6. Single-stage LED linear model

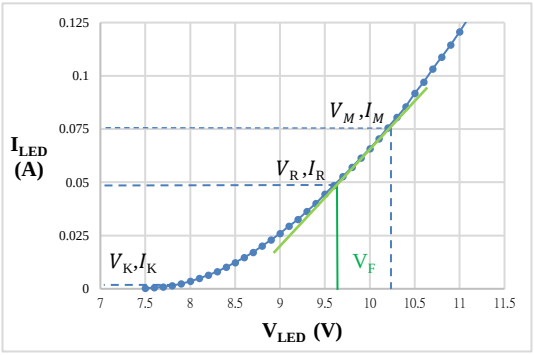

Figureure 7. I–V curve of the maximum and minimum operating point of the LED

Equation (5) presents the nonlinear LED current–voltage characteristic. For $V_F >> V_T$, (5) can be simplified as (6), where V_T is the thermal voltage, which is approximately 25 mV at room temperature.

$$I_F = I_{sat}(e^{\frac{q \cdot V_f}{n \cdot k \cdot T}} - 1) \quad (5)$$

I_F : forward current and V_F : forward voltage.

I_{sat} : saturation current or critical current of the diode, which equals the current when the voltage V_F exceeds V_T in the negative direction and is usually 10^{-12}A.

n: ideality factor of the diode, which falls between 1 and 2 for a silicon diode.

q : number of the electric charges of the electron (=1.62 • 10^{-19}).

k : Boltzmann constant (=1.38 • 10^{-23})

T : absolute temperature (=273+ room temperature)

V_T : Thermal Voltage of LED

$$I_F = I_{sat}(e^{\frac{V_f}{n \cdot V_T}}) \quad (6)$$

$$V_T = \frac{k \cdot T}{q} \quad (7)$$

Equation (8) is obtained by using the LED model presented in Fig. 6 and represents the relationship between the voltage across the LED and forward voltage of the LED, where r is the internal resistance of the LED. Equation (9) can be obtained by substituting (6) and (7) into (8).

$$V_F = V_{LED} - I_{LED} \cdot r \quad (8)$$

$$V_{LED} = n \cdot V_T \cdot \ln(\frac{I_F}{I_{sat}}) + I_F \cdot r \quad (9)$$

The maximum operating point (V_M, I_M), minimum operating point (V_K, I_K), and rated operating point (V_R, I_R) can be obtained from the datasheet of the luminaire. Fig. 7 presents the I–V curve marked with the aforementioned operating points. The rated and maximum operating points are subsequently connected to form a straight line; the internal resistance (r) parameter is obtained by calculating the slope of said line with (10):

$$r = \frac{V_M - V_R}{I_M - I_R} \quad (10)$$

The ideality factor (n) is obtained by substituting (10) into (9) to yield (11):

$$n = \frac{V_K - V_M - r \cdot (I_K - I_M)}{V_T \cdot \ln(\frac{I_K}{I_M})} \quad (11)$$

The saturation current (I_{sat}) is obtained by substituting the minimum operating point (V_M, I_M) into (6), as given by (12):

$$I_{sat} = \frac{I_K}{e^{\frac{V_K - r \cdot I_K}{n \cdot V_T}}} \quad (12)$$

$$I_F = I_{sat} \sum_{j=0}^{\infty} \frac{(\frac{V_{LED} - r \cdot I_F}{n \cdot V_T})^j}{j!} \quad (13)$$

To obtain an accurate I–V curve, the Taylor series is required to obtain the nonlinear load. The used equation is given by (13), where the unknown parameters are obtained from (10) – (12) and the forward current obtained from simulation is also substituted into the equation. Additionally, j denotes the number of levels. The simulated current varies with the number of levels set by the Taylor series.

4. System Simulation

4.1 Introduction Of The Simulation

The simulation software employed in this study is SIMetrix/SIMPLIS. Fig. 8 presents the flyback PFC circuit simulation framework, which contains the same main circuit as a regular flyback converter. In addition, the circuit established in this study contains a ZCD, which enables soft-switching of the switch, reduces loss, and improves overall efficiency of the system. The characteristic of this circuit is similar to that of the quasi-resonant flyback converter. Both switches are triggered when the voltage V_{ds} reaches the wave trough.

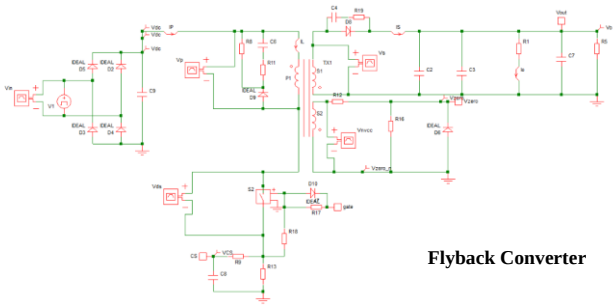

Figureure 8. Flyback PFC circuit simulation framework

Fig. 9 presents the SIMPLIS circuit control block module of PFC function and closed-loop feedback. The main control functions include four control blocks: 1. switch current sensor signal (CS), 2. closed-loop feedback signal (COMP), 3. ZCD function for the auxiliary winding of the transformer, and 4. COT control of PFC [17], [18].

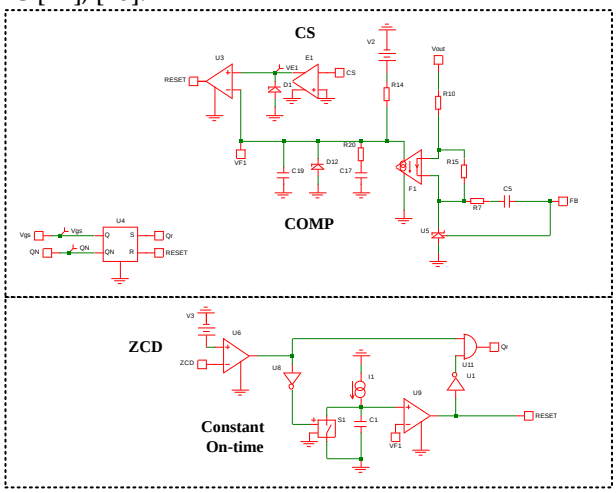

Figureure 9. PFC and closed-loop control circuits

4.2 Simulation Results

The LED model as the output load is referenced by Fig. 6 in Chapter III. Using this model in SIMPLIS simulation is to emulate the realistic LED I-V curve. The simulation conditions include full-range input voltage to demonstrate the system stability is well-performed and check the voltage and current of LED approximate to the Mathcad computation.

First, Figs. 10 and 11 show the whole system works under the normal operation conditions. The maximum output load of this system is 120W and the input voltage is set by 85V and 265 V individually. The input voltage and current are completely in phase and the output voltage across LED is kept at the rated voltage of 12 V. Figs. 12 and 13 show the current flowing through LED maintains at 0.1085A whether the input voltage is 85 V or 265 V. The simulation results prove the system is validated for a single-stage flyback PFC converter.

At next, in order to plot the simulated single-stage LEB I-V curve as shown in Fig. 14, the voltage on LED is designated as the independent variable and the current through LED naturally becomes the dependent variable. After repeating several times of simulation, the acquisition of data of LED voltage and current can plot the I-V curve, which can be a benchmark for experimental results afterwards.

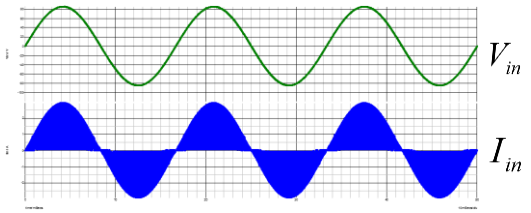

Figureure 10. Simulation of V_{in} and I_{in} (V_{in}=85 V)

(I_{in}:1A/div、V_{in}:20V/div、Time:10ms/div)

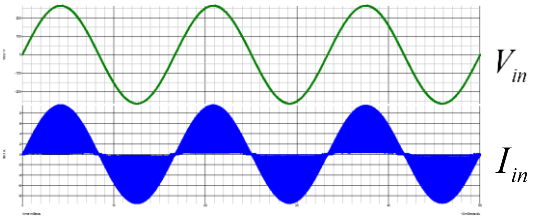

Figureure 11. Simulation of V_{in} and I_{in} (V_{in}=265 V)

(I_{in}:1A/div、V_{in}:50V/div、Time:10ms/div)

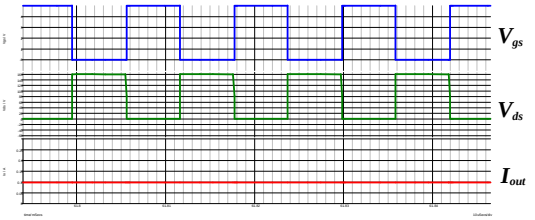

Figureure 12. Simulation of V_{gs}、V_{ds} and I_{out} (V_{in}=85 V; V_{out}=12 V)

(V_{gs}: 1.0V/div、V_{ds}:20V/div、I_{out}:0.05A/div、Time:10.0μs/div)

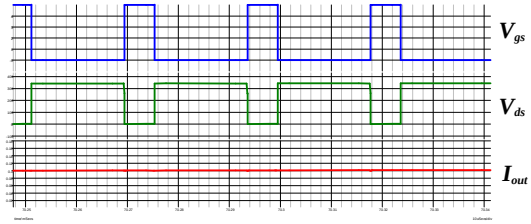

Figureure 13. Simulation of V_{gs}、V_{ds} and I_{out} (V_{in}=265 V; V_{out}=12 V)

(V_{gs}: 1.0V/div、V_{ds}:20V/div、I_{out}:0.02A/div、Time:10.0μs/div)

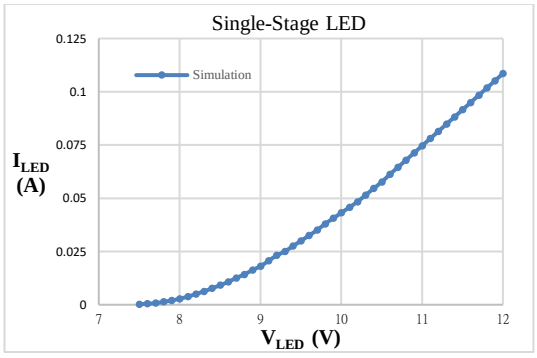

Figureure 14. Simulated results of single-stage LEDs

5. Waveform Measurements And Actual Data

5.1 Test Results Of The Circuit

Figs. 15, 16, 17, and 18 present the input voltage V_{in} and current I_{in} waveforms of the flyback LED driver operating under a full-load (120 W) condition. Four input voltages are chosen for testing, namely 85 V, 110 V, 220 V, and 265 V

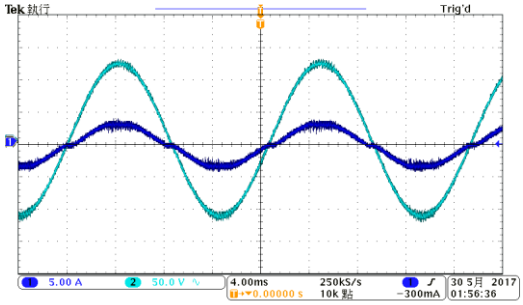

Figureure 15. Waveforms of V_{in} and I_{in} ($V_{in} = 85$ V)
($Ch1 = I_{in}$: 5A/div 、 $Ch2 = V_{in}$: 50V/div 、 Time: 4.0ms/div)

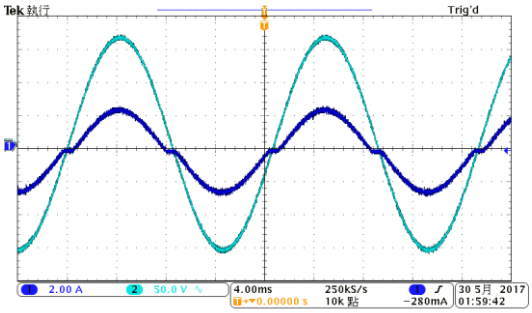

Figureure 16. Waveforms of V_{in} and I_{in} ($V_{in} = 110$ V)
($Ch1 = I_{in}$: 5A/div 、 $Ch2 = V_{in}$: 50V/div 、 Time: 4.0ms/div)

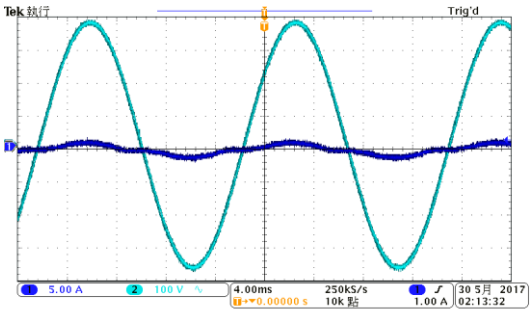

Figureure 17. Waveforms of V_{in} and I_{in} ($V_{in} = 220$ V)
($Ch1 = I_{in}$: 5A/div 、 $Ch2 = V_{in}$: 100V/div 、 Time: 4.0ms/div)

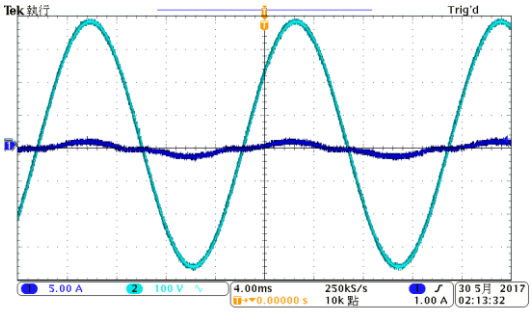

Figureure 18. Waveforms of V_{in} and I_{in} ($V_{in} = 265$ V)
($Ch1 = I_{in}$: 5A/div 、 $Ch2 = V_{in}$: 100V/div 、 Time: 4.0ms/div)

5.2 Comparison Of The Taylor Series Simulation And Actual Results

The data from the simulation with the Taylor series analysis and actual testing were illustrated as below. Figs. 19 and 20 present comparisons of the single-stage and multi-stage results, respectively. This method reduced the error to less than 3%. Figs. 21, 22, 23, 24, 25 and 26 present the simulation results with corrections by adding thermal parameters. With the thermal parameter correction, the overall system error was reduced to

less than 1.39%.

1) Comparison of single-stage and multi-stage simulations and actual testing results

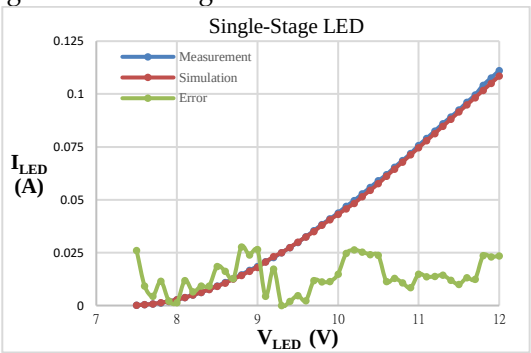

Figureure 19. Measured and simulated results of single-stage LEDs

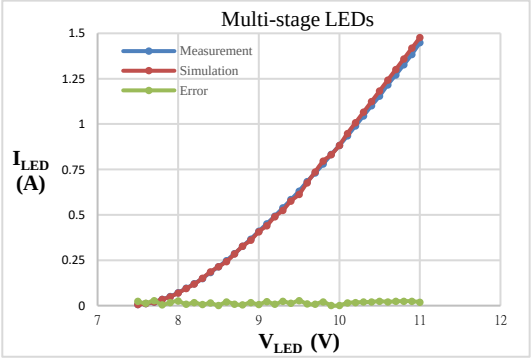

Figureure 20. Measured and simulated results of multi-stage LEDs (24units)

2) Comparison Of Simulation And Actual Testing Results Obtained After Thermal Correction

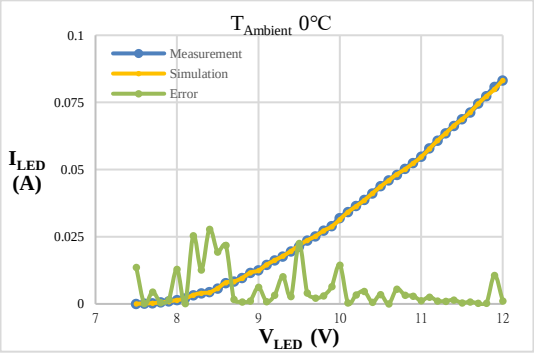

Figureure 21. Measured and simulated results at $T_{Ambient}$ 0℃

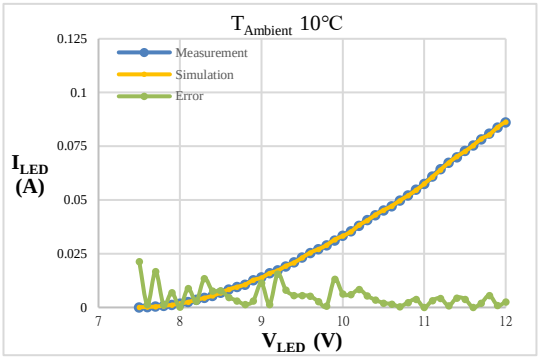

Figureure 22. Measured and simulated results at T Ambient 10℃

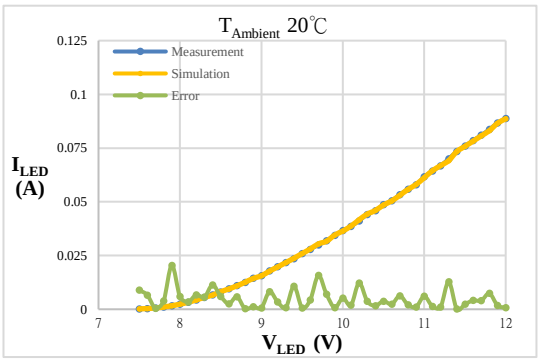

Figureure 23. Measured and simulated results at T Ambient 20℃

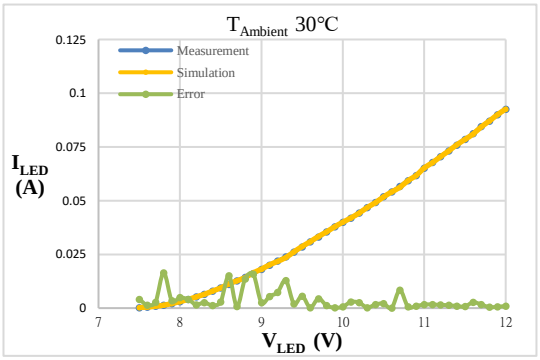

Figureure 24. Measured and simulated results at T Ambient 30℃

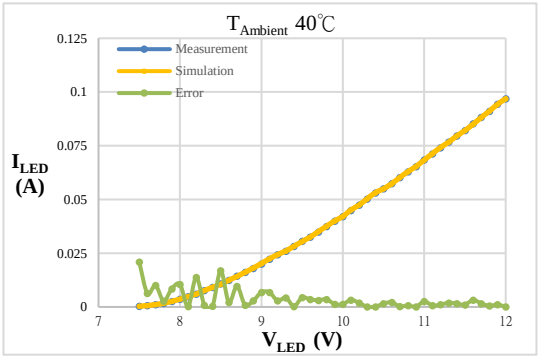

Figureure 25. Measured and simulated results at T Ambient 40℃

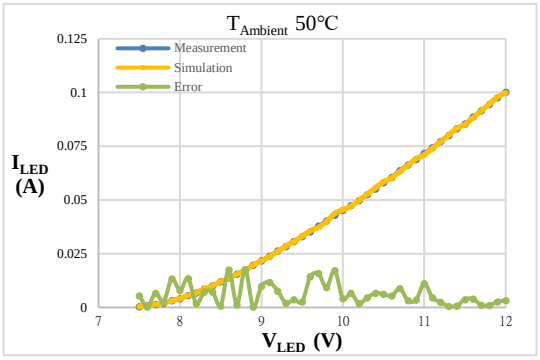

Figureure 26. Measured and simulated results at $T_{Ambient}$ 50℃

5. Conclusion

The Taylor series load simulation analysis established in this study together with the flyback LED driver could quickly obtain results for the actual circuit through simulations. Furthermore, the inclusion of thermal parameter adjustment could further increase the similarity between the system simulation and actual design to reduce error. Through the analysis in this study, products designed for use at different temperatures can establish the precise simulation module to predict their actual performance in order to simplify the circuit design process and meet demands for system safety, reliability, and adjustability. In addition, the power converter designed in this study can be used under a wide input voltage range (85-265 V), and the luminaire output is fit for 120-W LEDs for commercial lighting products. The present study first details an explicit analysis of the working principles of the LED driver and then uses mathematical models to derive equations and calculate the parameters of each device. The simulation software SIMPLIS was used to establish emulated power converter modules. The simulation results can precisely demonstrate the real waveform of each node in advance to improve the yield rate of the system design and reduce the time required for circuit debugging. Finally, the actual parameters are substituted into the prototype circuit to complete the circuit testing.

Acknowledgments: This work was supported by the National Science Council of Taiwan under Contract MOST 108-2221-E-011-082. The authors would like to thank Leadtrend Technology Corp. for the support on chip fabrication, measurement, and verifications.

Conflicts of Interest: The authors declare no conflict of interest.

References

1. R. N. Hall, G. E. Fenner, J. D. Kingsley, T. J. Soltys, and R. O. Carlson, “Coherent light emission from GaAs junctions,” Physical Review Letters., vol. 9, no. 9, pp. 366-368, Nov. 1962.
2. R. Lenk and C. Lenk, Practical Lighting Design With LEDs. Hoboken, NJ,USA: Wiley, 2011.
3. L. Feola, R. Langella, and A. Testa, “A new frequency approach for light flicker evaluation in electric power systems, ” EURASIP J. Adv. Signal Process., vol. 85, Mar. 2015.
4. Yong Deok Ahn, Sungwoo Bae, Suk-Ju Kang, "Power Controllable LED System with Increased Energy Efficiency Using Multi-Sensors for Plant Cultivation ", *Energies* 2017, *10*(10), 1607.
5. Zhou Yan, Qian Siyao, Qi Zhu, Liang Huang, Aiguo Patrick Hu, " A Simple Brightness and Color Control Method for LED Lighting Based on Wireless Power Transfer ", Access IEEE, vol. 6, pp. 51477-51483, 2018.
6. J. Cardes, D. Garc, L. a, L. E, et al, “Low Cost Intelligent LED Driver for Public Lighting Smart Grids,” in New Concepts in Smart Cities: Fostering Public and Private Alliances (SmartMILE), 2013 International Conference on, pp. 1-6, 2013.

7. Ray-Lee Lin, and Yi-Fan Chen, “Equivalent Circuit Model of Light-Emitting-Diode for System Analyses of Lighting Drivers,” IEEE Conference on IAS Annual meeting, pp. 1-5, 2009.
8. L. Bor-Ren, W. Ta-Chang, and C. Huann-Keng, “Novel AC Line Conditioner for Power Factor Correction,” IEEE Transactions on Aerospace and Electronic Systems, vol. 40, pp. 168-179, 2004.
9. Sri Lakshmi Nalla, H.L. Hess, K.M. Buck, E.J. Mentze, "Flyback converter with voltage control mode on chip for portable applications", IEEE Microelectronics and Electron Devices, pp. 80-83, 15–15 April 2005.
10. K. C. Juang, S. J. Chiang, W. M. Xiao, "A grid-tied flyback-based PV inverter with BCM variable frequency voltage mode control", Proc. Int. Symp. Intell. Signal Process. Commun. Syst., pp. 598-603, 2012.
11. J. S. Lai and D. Chen, “Design Consideration for Power Factor Correction Boost Converter Operating at the Boundary of Continuous Conduction Mode and Discontinuous Conduction Mode,” Proceeding of IEEE Applied Power Electronics Conference, pp.267-273, 1993.
12. R.-L. Lin, S.-Y. Liu, and H.-W. Chiang, “Optimal LED array combination for single-loop CCM boost driver,” Proc. IEEE Ind. Appl. Soc. Annu. Meeting (IAS), pp. 1-7, Oct. 2012.
13. R.-L. Lin, C.-C. Lee, and S.-Y. Liu, “Taylor series expression based equivalent circuit models of LEDs for analysis of LED driver system,” in Conf. Rec. IEEE IAS Annu. Meeting, pp. 1-7, Oct. 2011.
14. R.-L. Lin, S.-Y. Liu, C.-C. Lee, and Y.-C. Chang, “Taylor-seriesexpression-based equivalent circuit models of LED for analysis of LED driver system,” in IEEE Trans. Ind. Appl., vol. 49, no. 4, pp. 1854-1862, Jul./Aug. 2013.
15. R.-L. Lin and Y.-F. Chen, “Equivalent circuit model of light-emittingdiode for system analyses of lighting drivers,” in conf. Rec. IEEE 44th IAS Annu. Meeting, pp. 1-5, 2009.
16. E. F. Schubert, Light-Emitting Diodes. Cambridge, U.K.: Cambridge Univ. Press, 2003.
17. C. Tzuen-Lih, L. Li-Hsiang, H. Ching-Nan, C. Yu-Lun, and K. Jao-Hwa, “High Power Factor Flyback Converter for LED Driver with Boundary Conduction Mode Control,” in Proc. 5th IEEE Conf. Ind. Electron. Appl., pp. 2088-2093, 2010-Jun.-1517.
18. Liu Y., Yin S., Pan X., Wang H., Wang G.; Peng J., "Effects of Nonlinearity in Input Filter on the Dynamic Behavior of an Interleaved Boost PFC Converter ", *Energies* 2017, *10*(10), 1530.